Observer-based Grid Voltage Disturbance Rejection for Grid Connected Voltage Source PWM Converters with Line Side LCL filters

Nils Hoffmann*, Michael Hempel*, Michael C. Harke** and Friedrich W. Fuchs*

*Institute for Power Electronics and Electrical Drives
Christian-Albrechts-University of Kiel
D-24143 Kiel, Germany
nho@tf.uni-kiel.de

**Danfoss Power Electronics
Loves Park, IL, 61111 USA
michaelh@danfoss.com

***Abstract*—This work presents an extended disturbance observer design for grid voltage disturbance rejection of voltage source PWM converters with LCL filters. The proposed observer design leads to a cascaded extended disturbance observer using either the converter side current or the line side current for feedback. Theoretical aspects including the LCL filter system observability, observer pole placement strategy and practical implementation are discussed to achieve an observer formulation. The analysis presented is based on a fully analytical observer formulation in the discrete time-domain. The discrete state-space modeling of the LCL filter dynamics is discussed and a step-by-step observer formulation is presented. The theoretical analysis is verified on a 22 kW laboratory type adjustable speed drive system where the control algorithms are implemented on a dSpace system. The analysis reveals excellent disturbance rejection capabilities of the proposed cascaded extended disturbance observer design for both feedback cases.**

NOMENCLATURE

$\underline{X}$	Space-vector of three-phase System $X_{a,b,c}$
$\underline{X}^{\alpha\beta}$	Space-vector in stationary ($\alpha\beta$) reference frame
$\underline{X}^{dq}$	Space-vector in rotating (dq) reference frame
${}^{h}\underline{X}$	h^{th} harmonic of $\underline{X}$

I. INTRODUCTION

During the last years distributed power generation for renewable energy sources has become one of the major topics in power electronic engineering. The rapidly growing amount of renewable energy sources connected to the main electric distribution system leads to an increased amount of converters feeding power to the grid [1], [2]. These converters are hereto referred to as active in-feed converters (AICs).

To reduce the high-order harmonic current distortion caused by the AIC switching transitions, various line filters are used for grid connection. An appropriate choice of the related line filter depends on several design criteria including (but limited to) the AIC hardware topology, the average switching frequency, performance requirements, the modulation strategy and cost. A widely used cost and performance effective line filter topology for voltage source AICs is the LCL type line filter [3]. In addition to the attenuation of the high-order switching voltage harmonics (greater than the filters resonance frequency), the LCL filter has a reduced reactive power consumption and a lower voltage drop over the filter inductance in active power in-feed operation compared to conventional L-type line filters.

Voltage quality is one of the most important issues when connecting a renewable energy source via an AIC to the grid [4]-[7]. A reduced supply voltage quality often results from finite grid impedance, the presence of unbalanced or single-phase loads, and harmonic current distortions generated by nonlinear loads such as diode-bridge connected loads, thyristor-bridge connected loads or switched-mode power supplies [8]. A new trend is to use the grid connected AIC to mitigate the supply voltage unbalance and harmonics in addition to the fundamental power in-feed [9]-[12]. The emission of unbalanced and harmonic currents for grid connected renewable energy sources is strictly limited by international standards and grid code requirements to avoid further voltage quality degradation [13], [14].

Distorted supply voltage conditions containing a high amount of unbalanced and low-order harmonic voltage contents affect the operational behavior and the performance of grid connected AICs. More precisely, these non-ideal supply voltage waveforms act as disturbances to the current control of grid connected pulse-width modulated (PWM) AICs. To meet the aforementioned international standards and grid-code requirements, proper disturbance rejection of the current control to voltage unbalances and low-order harmonics is required. The goal is to achieve balanced current waveforms with a reduced content of low-order current harmonics at the AIC's connection point to the main electric distribution grid even under highly distorted supply voltage conditions.

Different approaches have been published to achieve good voltage disturbance rejection for current controlled grid connected PWM AICs [4], [15]-[20]. Two widely used methods use either an observer-based voltage feed-forward [4], [15] or additional parallel resonant current controllers added [16] to the fundamental current control. Both methods have distinguished features and the appropriate choice of the voltage disturbance rejection method depends often on additional boundary conditions such as the available sensors and their

978-1-4673-0803-8/12/$31.00 ©2012 IEEE

location, the available computational power or implementation complexity and tuning of the disturbance rejection method.

This work focuses on observer-based voltage disturbance rejection methods. The voltage rejection is achieved by adding a voltage feed-forward term including the observed voltage unbalances and harmonics to the fundamental current control of the grid connected AIC. In [18], the principle for an observer-based voltage rejection was presented in detail for grid connected AICs with L-type line filters. However, when LCL line filters are used for the grid connection of AICs, the study presented in [4] reveals a more complex observer formulation to achieve proper voltage disturbance rejection.

This work aims to contribute to the knowledge of disturbance observer design for grid connected PWM AICs with LCL line filters. First an analytical derived model of the sampled three-phase LCL system is used for the disturbance observer design. Then, a transformation law is presented to transform the analytical observer formulation from the stationary *(αβ)* reference frame to the rotating *(dq)* reference frame. Finally, the disturbance observer design is discussed and experimentally analyzed for both the feedback of the converter side current and the feedback of the line-side current as the input of the disturbance observer.

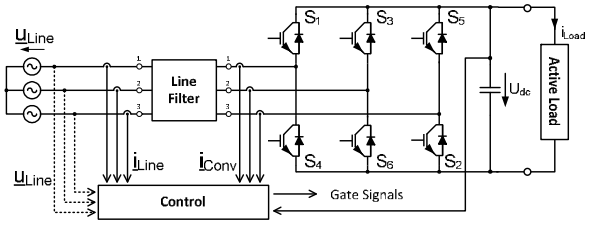

Fig. 1 Block diagram of two-level voltage source grid connected AIC

II. System Description and Sensor Restrictions

Figure 1 is the block diagram of a two-level voltage source AIC connected through a line filter to the grid. The renewable energy source is modeled as an active load. The LCL filter is illustrated in Fig. 2. The filter is composed of a converter side inductor L_c, a line side inductor L_g and a filter capacitor C_f. The LCL filter considered here is designed to meet the harmonic-current characteristics for AICs defined by the German VDN-requirements [21].

Two different current feedback cases are explored for the proposed extended disturbance observer (eDO) design: line side current sensors and converter side current sensors, Fig. 1. Only one set of current sensors is used at a time with respect to the observer design under study. The line side voltage sensors are shown in dashed lines, highlighting the principle of the proposed eDO design.

When the eDO is used in combination with line side voltage sensors, the observer is used to overcome the measurement time delays introduced by the analog-to-digital signal conversion. This sample-and-hold behavior introduces phase error to the sampled voltage waveforms which is significant for systems operating at low sampling frequencies relative to the fundamental frequency. Further, the inherent filtering nature of the eDO can be used to overcome the need of adding additional voltage filters to the control loops.

The proposed eDO can also be used when no line voltage sensors are available. The eDO can be used in combination with a virtual flux estimator [22] to achieve a proper line voltage disturbance rejection. In this case, the principle of virtual flux is used to extract the fundamental grid voltage phase angle from the measured DC-link voltage waveform. Then, the eDO can be used to reconstruct the positive and negative fundamental voltage waveforms as well as the low-order harmonic voltage waveforms to achieve proper voltage disturbance rejection for the current controller.

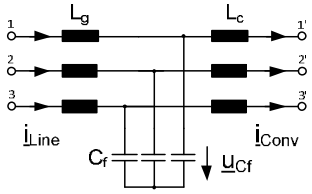

Fig. 2 Circuit diagram of LCL filter

III. State-Space Model of an LCL Filter

The eDO design is done based on an ideal state-space model of the LCL filter, Fig. 2. To simplify the observer formulation, the losses of the filter components are not considered.

A. State-space model in the continuous time-domain

Based on Kirchhoff's laws, the state-space model of the loss-free LCL filter is derived. The LCL state vector is chosen according to (1). The resulting LCL state space model is presented in (2).

$$\underline{x}_{LCL}^{\alpha\beta} = \left[\underline{I}_{Line}^{\alpha\beta}(t) \quad \underline{I}_{Conv}^{\alpha\beta}(t) \quad \underline{U}_{Cf}^{\alpha\beta}(t)\right]^T \tag{1}$$

$$\frac{d}{dt}\begin{bmatrix}\underline{I}_{Line}^{\alpha\beta}(t)\\ \underline{I}_{Conv}^{\alpha\beta}(t)\\ \underline{U}_{Cf}^{\alpha\beta}(t)\end{bmatrix} = \overbrace{\begin{bmatrix}0 & 0 & -\frac{1}{L_g}\\ 0 & 0 & \frac{1}{L_c}\\ \frac{1}{C_F} & -\frac{1}{C_F} & 0\end{bmatrix}}^{=A} \overbrace{\begin{bmatrix}\underline{I}_{Line}^{\alpha\beta}(t)\\ \underline{I}_{Conv}^{\alpha\beta}(t)\\ \underline{U}_{Cf}^{\alpha\beta}(t)\end{bmatrix}}^{\underline{x}} + \underbrace{\begin{bmatrix}0 & \frac{1}{L_g}\\ -\frac{1}{L_c} & 0\\ 0 & 0\end{bmatrix}}_{B} \underbrace{\begin{bmatrix}\underline{U}_{Conv}^{\alpha\beta}(t)\\ \underline{U}_{Line}^{\alpha\beta}(t)\end{bmatrix}}_{\underline{u}} \tag{2}$$

$$\underline{y}(t) = \underline{c}^T \underline{x}_{LCL}^{\alpha\beta}(t)$$

B. State-space model in the discrete time-domain

The observer formulation is presented in the discrete time-domain taking advantage of the straight forward modeling when additional time delays are considered. Taking the characteristic zero-order hold behavior of the analog-to-digital signal conversion into account, the equivalent state space model in the discrete time-domain is derived using the transformation laws presented in (3)-(5).

$$A_d = e^{A\,T_s} \tag{3}$$

$$B_d = \{A_d - I\}A^{-1}B \tag{4}$$

$$\underline{c}_d{}^T = \underline{c}^T \tag{5}$$

The resulting state-space model is presented in (6) and the related coefficients are summarized in Table III of the Appendix.

$$\begin{bmatrix} \underline{I}_{Line}^{\alpha\beta}(k+1) \\ \underline{I}_{Conv}^{\alpha\beta}(k+1) \\ \underline{U}_{Cf}^{\alpha\beta}(k+1) \end{bmatrix} = \begin{bmatrix} a_{11} & a_{12} & a_{13} \\ a_{21} & a_{22} & a_{23} \\ a_{31} & a_{32} & a_{33} \end{bmatrix} \begin{bmatrix} \underline{I}_{Line}^{\alpha\beta}(k) \\ \underline{I}_{Conv}^{\alpha\beta}(k) \\ \underline{U}_{Cf}^{\alpha\beta}(k) \end{bmatrix} + \begin{bmatrix} b_{11} & b_{12} \\ b_{21} & b_{22} \\ b_{31} & b_{32} \end{bmatrix} \begin{bmatrix} \underline{U}_{Conv}^{\alpha\beta}(k) \\ \underline{U}_{Line}^{\alpha\beta}(k) \end{bmatrix} \tag{6}$$

$$\underline{y}(k) = \underline{c}^T \underline{x}_{LCL}^{\alpha\beta}(k)$$

IV. Discrete Time-Domain Observer Formulation

In the following paragraphs a step-by-step formulation of the eDO is presented.

A. State observer (SO) formulation

Based on the state-space model for the LCL filter in the discrete time-domain (6), a state observer (SO) is derived. The SO takes advantage of the fact that the system states can be estimated from the measurement of certain system outputs. To reduce the error in the estimated system states due to model mismatch and parameter estimation errors, the observed (estimated) and the measured system outputs are fed back to the estimated system states. By adjusting the coefficients of the feedback gain vector, referred to here as L_p, the dynamics and performance of the closed-loop state observer can be adjusted to meet certain design criteria.

The state-space model of the observer is defined by (7) and (8). Here, the subscript *obs* refers to the estimated states of the SO.

$$\underline{x}_{obs}(k+1) = A\underline{x}_{obs}(k) + L_p[y(k) - y_{obs}(k)] + Bu_{obs}(k) \tag{7}$$

$$y_{obs}(k) = \underline{c}^T \underline{x}_{obs}(k) \tag{8}$$

The dynamics of state estimation error $\underline{x}_{err}$ of the closed loop state observer formulation are derived as (9).

$$\underline{x}_{err}(k+1) = \underline{x}(k+1) - \underline{x}_{obs}(k+1) = \left(A - L_p\underline{c}^T\right)\underline{x}_{err}(k) \tag{9}$$

Two important criteria for the presented SO formulation are mentioned at this point. First, the input vector of the observer u_{obs} is considered to be known at each sampling instant *k*. In the case of the LCL filter, this is the line voltage and the converter voltage. Thus, further manipulation of the observer formulation is necessary to estimate the line voltage waveforms leading to a disturbance observer (DO) formulation. Second, the system states can be observed if the system is observable.

B. Observability

Different measured system outputs can used for observer formulation. To analyze the observability of the LCL filter for different system output measurements, the simplified Kalman criterion [23] is used. The analysis of the discrete state observer formulation reveals that the (loss-free) LCL filter

- is observable for the measurement of the line side currents,
- is observable for the measurement of the converter side currents, and
- is not observable for the measurement of the filter capacitor voltages.

Therefore, the measurement of the filter capacitor voltages is not considered for further analysis.

C. Including PWM time delay in the state observer

The time delay caused by the converter sampling and PWM update calculation process is considered for the observer design. Considering that the time delay is limited to one sampling instant, the converters reference voltage $u_{conv,ref}$ is adjusted by the PWM algorithm in the following sampling instant (10).

$$\underline{U}_{Conv,ref}^{\alpha\beta}(k) = \underline{U}_{Conv}^{\alpha\beta}(k+1) \tag{10}$$

The state space model of the LCL-filter system including the effect of the time delay is formulated in (11).

$$\begin{bmatrix} \underline{I}_{Line}^{\alpha\beta}(k+1) \\ \underline{I}_{Conv}^{\alpha\beta}(k+1) \\ \underline{U}_{Cf}^{\alpha\beta}(k+1) \\ \underline{U}_{Conv}^{\alpha\beta}(k+1) \end{bmatrix} = \begin{bmatrix} & A_d & & b_{11} \\ & & & b_{21} \\ & & & b_{31} \\ 0 & 0 & 0 & 0 \end{bmatrix} \begin{bmatrix} \underline{I}_{Line}^{\alpha\beta}(k) \\ \underline{I}_{Conv}^{\alpha\beta}(k) \\ \underline{U}_{Cf}^{\alpha\beta}(k) \\ \underline{U}_{Conv}^{\alpha\beta}(k) \end{bmatrix} + \begin{bmatrix} 0 & b_{12} \\ 0 & b_{22} \\ 0 & b_{32} \\ 1 & 0 \end{bmatrix} \begin{bmatrix} \underline{U}_{Conv,ref}^{\alpha\beta}(k) \\ \underline{U}_{Line}^{\alpha\beta}(k) \end{bmatrix} \tag{11}$$

D. Disturbance observer (DO) formulation

The presented SO formulation is further manipulated to include the line voltages leading to the disturbance observer (DO) formulation presented in (12).

$$\begin{bmatrix} \underline{I}_{Line}^{\alpha\beta}(k+1) \\ \underline{I}_{Conv}^{\alpha\beta}(k+1) \\ \underline{U}_{Cf}^{\alpha\beta}(k+1) \\ \underline{U}_{Conv}^{\alpha\beta}(k+1) \\ \underline{U}_{Line}^{\alpha\beta}(k+1) \end{bmatrix} = \begin{bmatrix} & A_d & & & B_d \\ 0 & 0 & 0 & 0 & 0 \\ 0 & 0 & 0 & 0 & 0 \end{bmatrix} \begin{bmatrix} \underline{I}_{Line}^{\alpha\beta}(k) \\ \underline{I}_{Conv}^{\alpha\beta}(k) \\ \underline{U}_{Cf}^{\alpha\beta}(k) \\ \underline{U}_{Conv}^{\alpha\beta}(k) \\ \underline{U}_{Line}^{\alpha\beta}(k \end{bmatrix} + \begin{bmatrix} 0 \\ 0 \\ 0 \\ 1 \\ 0 \end{bmatrix} \underline{U}_{Conv,ref}^{\alpha\beta}(k) \tag{12}$$

The advantage of the DO formulation is that by adding the line voltage to the system states, the DO input vector depends only on the known reference value of the converter output voltage. The analysis of the observability reveals no changes to the results already presented in section IV. B.

E. Extended disturbance observer (eDO) formulation

To achieve voltage disturbance rejection to unbalanced line voltage and low-order voltage harmonics, the presented DO formulation is further manipulated resulting in an extended disturbance observer (eDO) formulation. In [15] the underlying principles of including unbalanced line voltage and low-order harmonics are presented for an L-type filter system. These results are adapted for the LCL type filter system. A sinusoidal disturbance, where the h^{th} harmonic order of the fundamental

component is considered for disturbance rejection, is modeled in continuous time domain using (13).

$$\frac{d}{dt}\begin{bmatrix} {}^{h}\underline{U}_{Line}^{\alpha\beta}(t) \\ d/dt\ {}^{h}\underline{U}_{Line}^{\alpha\beta}(t) \end{bmatrix} = \begin{bmatrix} 0 & 1 \\ -h^2\omega_{Line} & 0 \end{bmatrix}\begin{bmatrix} {}^{h}\underline{U}_{Line}^{\alpha\beta}(t) \\ d/dt\ {}^{h}\underline{U}_{Line}^{\alpha\beta}(t) \end{bmatrix} \tag{13}$$

The discrete time-domain equivalent state model formulation of this sinusoidal disturbance is presented by (14). The related coefficients are summarized in Table IV of the Appendix.

$$\begin{bmatrix} {}^{h}\underline{U}_{Line}^{\alpha\beta}(k+1) \\ {}^{h}\underline{U}_{Line}^{\alpha\beta}(k+2) \end{bmatrix} = \begin{bmatrix} s_{11} & s_{12} \\ s_{21} & s_{22} \end{bmatrix}\begin{bmatrix} {}^{h}\underline{U}_{Line}^{\alpha\beta}(k) \\ {}^{h}\underline{U}_{Line}^{\alpha\beta}(k+1) \end{bmatrix} \tag{14}$$

This disturbance model is included to the DO formulation (12) leading to the eDO formulation (15).

$$\begin{bmatrix} \underline{I}_{Line}^{\alpha\beta}(k+1) \\ \underline{I}_{Conv}^{\alpha\beta}(k+1) \\ \underline{U}_{Cf}^{\alpha\beta}(k+1) \\ \underline{U}_{Conv}^{\alpha\beta}(k+1) \\ \underline{U}_{Line}^{\alpha\beta}(k+1) \\ {}^{h}\underline{U}_{Line}^{\alpha\beta}(k+1) \\ {}^{h}\underline{U}_{Line}^{\alpha\beta}(k+2) \end{bmatrix} = \overbrace{\begin{bmatrix} & & & b_{12} & 0 \\ A_d & & B_d & b_{22} & 0 \\ & & & b_{32} & 0 \\ 0 & \dots & 0 & 0 & 0 \\ \vdots & & & 0 & 0 \\ & & \vdots & s_{11} & s_{12} \\ 0 & \dots & 0 & s_{21} & s_{22} \end{bmatrix}}^{:=A_d}\begin{bmatrix} \underline{I}_{Line}^{\alpha\beta}(k) \\ \underline{I}_{Conv}^{\alpha\beta}(k) \\ \underline{U}_{Cf}^{\alpha\beta}(k) \\ \underline{U}_{Conv}^{\alpha\beta}(k) \\ \underline{U}_{Line}^{\alpha\beta}(k \end{bmatrix} + \underbrace{\begin{bmatrix} 0 \\ 0 \\ 0 \\ 1 \\ 0 \\ 0 \end{bmatrix}}_{:=\underline{b}_d}\underline{U}_{Conv,ref}^{\alpha\beta}(k) \tag{15}$$

The analysis of the observability reveals no changes to the results already presented in section IV. B.

F. Rotating (dq) reference frame observer formulation

Based on the observer formations in the stationary *(αβ)* reference frame, the related observer formulations in the rotating (dq) reference frame are calculated using the transformation laws presented in Appendix B. It is assumed that the line voltage angular frequency ω_{line} is (almost) constant.

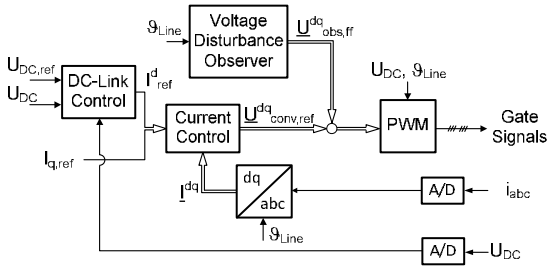

Fig. 3 Control diagram with the proposed disturbance observer-based voltage feed-forward

V. Observer-Based Grid Voltage Disturbance Rejection Implementation

The proposed eDO for voltage disturbance rejection can be used in two ways. First, when the line-voltages are measured, the eDO is used to overcome the measurement time delays introduced by the analog-to-digital signal conversion and the inherent filtering nature is used to eliminate the need of adding additional voltage filters to the control loops. Second, when line-voltages are not measured, the eDO can be used in combination with a virtual flux estimator to achieve a proper line voltage disturbance rejection.

In Fig. 3 the control block diagram of the grid connected PWM voltage source converter is presented. The control consists of cascaded control loops with an outer DC-link voltage control and an inner current control where the control variables are transformed to the rotating (dq) reference frame. The transformation angle is related to the line voltage phase angle. This control scheme is referred to as "voltage-oriented control".

The eDO is added to the control loops applying an observed feed-forward voltage to the commanded reference voltage. If the observed line voltage waveforms would be added at this point, a poor line voltage distortion rejection performance would result because the filter capacitor dynamics have not been considered. An ideal disturbance rejection of the line voltage disturbances to the line side currents is achieved when the disturbance voltages at the line side are equal to the voltage waveforms of the filter capacitors. To overcome these issues, two possible approaches can be used: the eDO can be reformulated introducing a sinusoidal disturbance state-space model for the filter capacitor waveforms or a cascaded extended disturbance observer (ceDO) approach can be used to estimate to voltage disturbances of the capacitor voltages. The ceDO approach is chosen because it results in straight forward tuning and design guidelines.

A. Cascaded extended disturbance observer formulation to achieve harmonic-free and balanced line-currents

In Fig. 2 the block diagram of the loss-free LCL filter is presented. To achieve an ideal line voltage disturbance rejection, the voltages in the filter capacitor have to be equal to the considered line voltage disturbance. This leads to the disturbance voltage compensation conditions formulated in (16) and (17).

$$\underline{U}_{C_f}^{\alpha\beta}(t) = \underline{U}_{Line}^{\alpha\beta}(t) \tag{16}$$

$$\underline{I}_{C_f}^{\alpha\beta}(t) = \underline{I}_{Conv}^{\alpha\beta}(t) \tag{17}$$

Based on these conditions for disturbance voltage compensation, the underlying state-space model in the continuous time-domain is derived (18).

$$\frac{d}{dt}\begin{bmatrix} \underline{I}_{Conv}^{\alpha\beta}(t) \\ \underline{U}_{Line}^{\alpha\beta}(t) \end{bmatrix} = \begin{bmatrix} 0 & 1/L_c \\ -1/C_f & 0 \end{bmatrix}\begin{bmatrix} \underline{I}_{Conv}^{\alpha\beta}(t) \\ \underline{U}_{Line}^{\alpha\beta}(t) \end{bmatrix} + \begin{bmatrix} -1/L_c \\ 0 \end{bmatrix}\underline{U}_{Conv}^{\alpha\beta}(t) \tag{18}$$

Following the same principles that have already been presented during the eDO formulation, the state space-model of the second extended disturbance observer is formulated in the discrete time-domain (19) where the coefficients are summarized in the Table IV of the Appendix.

$$\begin{bmatrix} \underline{I}_{Conv}^{\alpha\beta}(k+1) \\ \underline{U}_{Line}^{\alpha\beta}(k+1) \\ \underline{U}_{Conv}^{\alpha\beta}(k+1) \\ {}^{h}\underline{U}_{Line}^{\alpha\beta}(k+1) \\ {}^{h}\underline{U}_{Line}^{\alpha\beta}(k+2) \end{bmatrix} = \overbrace{\begin{bmatrix} a'_{11} & a'_{12} & b'_1 & a'_{12} & 0 \\ a'_{21} & a'_{22} & b'_2 & a'_{22} & 0 \\ 0 & 0 & 0 & 0 & 0 \\ 0 & 0 & 0 & s_{11} & s_{12} \\ 0 & 0 & 0 & s_{21} & s_{22} \end{bmatrix}}^{:=A'_d} \begin{bmatrix} \underline{I}_{Conv}^{\alpha\beta}(k) \\ \underline{U}_{Line}^{\alpha\beta}(k) \\ \underline{U}_{Conv}^{\alpha\beta}(k) \\ {}^{h}\underline{U}_{Line}^{\alpha\beta}(k) \\ {}^{h}\underline{U}_{Line}^{\alpha\beta}(k) \end{bmatrix} + \underbrace{\begin{bmatrix} 0 \\ 0 \\ 1 \\ 0 \\ 0 \end{bmatrix}}_{:=\underline{b}'_d} \underline{U}_{Conv,ref}^{\alpha\beta}(k) \tag{19}$$

To simplify the notation used for the proposed ceDO approach, this second extended disturbance observer will be referred to as a compensation observer.

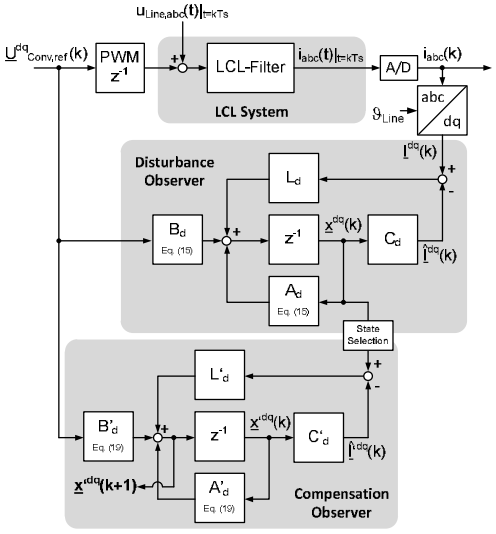

Fig. 4 Block diagram of proposed cascaded extended disturbance observer

B. Cascaded extended disturbance observer implementation

A ceDO formulation is proposed to achieve proper line voltage disturbance rejection for the line current of a LCL filter system. The ceDO formulation consists of two extended observers. The first extended disturbance observer is used to extract the sinusoidal line-voltage disturbances from either the measured line current or the measured converter current and the commanded converter output voltage. A second compensation observer is introduced to incorporate the dynamics of the filter capacitor voltages into the disturbance rejection of the line currents. In Fig. 4 the block diagram of the proposed ceDO is illustrated. A state selector is added to the ceDO block diagram because only the state variables needed from the disturbance observer are used for the compensation observer error correction.

VI. Observer Design and Pole-Placement Guidelines

Two measurement cases are considered: the measurement of the line side current or the measurement of the converter side current. The analysis is done for a generic h^{th} harmonic voltage disturbance.

A. Choice of the parameter h

The proposed ceDO can be implemented in two different reference frames: the stationary (αβ) reference frame or the rotating (dq) reference frame. In Table I the transformation of characteristic harmonic voltage contents from the $\alpha\beta$- to the dq-reference frame is summarized. A benefit of choosing the rotating *(dq)* reference system over the stationary ($\alpha\beta$) reference system for ceDO implementation is that the parameter h can be chosen to efficiently reduce the complexity -and thus the computational burden- of the ceDO implementation by rejecting two voltage disturbances in the same time.

TABLE I
HARMONIC SEQUENCES IN THE αβ– AND DQ-FRAME

reference frame			
stationary (αβ)	rotating (dq)	stationary (αβ)	rotating (dq)
1^{neg}/h=1	2^{neg}/h=2	7^{pos}/h=7	6^{pos}/h=6
3^{zero}/h=3	2^{pos}/h=2	11^{neg}/h=11	12^{neg}/h=12
5^{neg}/h=5	6^{neg}/h=6	13^{pos}/h=13	12^{pos}/h=12

'zero'- zero sequence, 'pos'- positive sequence, 'neg' – negative sequences

B. Pole placement for different current measurements

In Fig. 5 the chosen pole placement strategy for the observer considering measurement of the converter side current is illustrated for both the disturbance and compensation observers. Fig. 6 illustrates the pole placement strategy of the measurement of the line side current case. The open-loop observer poles and zeros are presented in black color and the closed-loop observer poles and zeros are presented in red. The same pole placement strategy is chosen for both current measurements cases.

The open-loop disturbance observer consists of six poles that can be positioned by providing a proportional feedback vector. Ackermann's formula is used for the pole placement for each of the possible measurement inputs of the disturbance observer. The proportional feedback vector L_p is derived to achieve the closed-loop disturbance observer poles presented in (20).

$$\begin{aligned} p_{1/2}&: \quad f_{p1/2} = \frac{3}{5} f_{res,LCL} \quad D_{p1/2} = \frac{3}{5} \\ p_{3/4}&: \quad f_{p3/4} = h\, f_{Line} \quad D_{p3/4} = \frac{9}{10} \\ p_5&: \quad f_{p5} = \frac{4}{5}\, h\, f_{Line} \quad D_{p5} = 1 \\ p_6&: \quad f_{p6} = \frac{4}{3}\, h\, f_{Line} \quad D_{p6} = 1 \end{aligned} \tag{20}$$

$$\begin{aligned} p'_{1/2}&: \quad Re\{p'_{1/2}\} = Re\{p_{1/2}\} - 0.03 \\ &\qquad Im\{p'_{1/2}\} = Im\{p_{1/2}\} \\ p'_{3/4}&: \quad Re\{p'_{3/4}\} = Re\{p_{3/4}\} - 0.03 \\ &\qquad Im\{p'_{3/4}\} = Im\{p_{3/4}\} \\ p'_5&: \quad Re\{p'_5\} = Re\{p_6\} - 0.03 \\ &\qquad Im\{p'_5\} = Im\{p_6\} \end{aligned} \tag{21}$$

The proposed disturbance observer pole placement strategy presents a tradeoff between the achievable dynamics of the

disturbance observer and the minimum stability margins to guarantee an appropriate robustness in relation to parameter uncertainties and model mismatches. The proposed pole placement strategy results in a phase margin of *26°* and a gain margin of *5* dB.

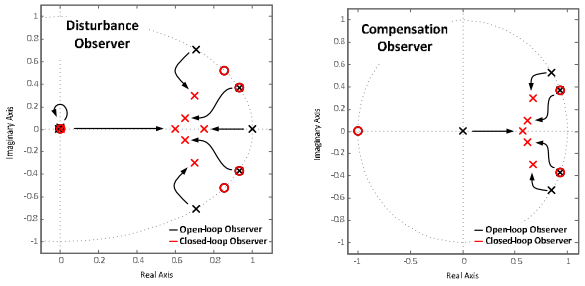

(a) (b)

Fig. 5 Pole placement strategies for (a) eDO and (b) ceDO using converter side current measurement

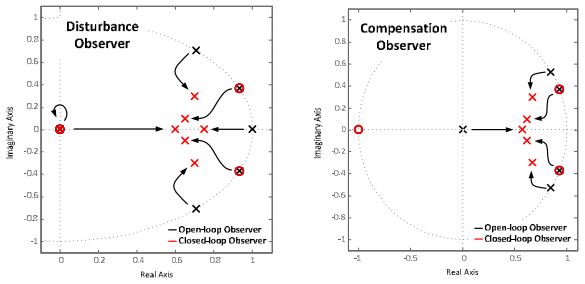

(a) (b)

Fig. 6 Pole placement strategies for (a) eDO and (b) ceDO using line side current as observer input

A cascaded observer approach is used to achieve proper voltage disturbance rejection. Based on the principles of cascaded control-loop design, the compensation observer dynamics are chosen to be faster than the disturbance observer dynamics. To achieve this goal, the fastest poles of the disturbance observer are identified and the real-part of these poles is reduced whereas the imaginary potion is left unchanged (21). The proposed pole placement strategy results in a phase margin of *30°* and a gain margin of *6* dB.

VII. Experimental Results

Experimental tests are carried out to validate the theoretical analysis under laboratory conditions. A *22* kVA laboratory test setup is used. The setup consists of a two- level back-to-back voltage source converter with an LCL filter. The system parameters are summarized in Table II. To emulate active load conditions, an interior permanent-magnet synchronous machine (PMSM) connected to a four-quadrant converter-fed DC load machine is used. The motor speed of the PMSM is set to *1500* r/min. The load torque is adjusted by the DC load-machine to maintain *5* % of the nominal power in power generation mode and a (inductive) reactive power of *5* kVA is fed into the grid. The control is implemented on a dSPACE DS1006 system.

TABLE II
EXPERIMENTAL SYSTEM PARAMETERS

Symbol	Quantity	Value (per unit)
U_{LL}	Line-to-Line Voltage (rms)	*400 V (1.0)*
U_{DC}	DC-link voltage	*700 V (1.75)*
ω	Angular grid frequency	*2π 50 Hz (1.0)*
I_L	Nominal line current (rms)	*31.0 A (1.0)*
L_g	Grid side filter inductance	*2 mH (0.086)*
L_c	Converter side filter inductance	*2 mH (0.086)*
C_f	Filter capacitance	*64.8 µF (0.148)*
C_{DC}	DC-link capacitance	*2200 µF (5.0)*
f_{con}/f_{switch}	Control/Switching frequency	*5 / 2.5 kHz (100 / 50)*

A. Disturbance rejection in steady-state conditions

To study the steady state voltage disturbance rejection, three experiments are carried out. The lab facility's actual grid voltage waveforms are used for the experiments. As it can be seen from Fig. 7 (a)/(b), the grid voltages contain a high amount of 5th and 7th harmonic voltages (5th harmonic voltage: *3.6* %, 7th harmonic voltage: *1.2* %).

First, the grid connected AIC is controlled using only the fundamental current control without any additional disturbance rejection added. Figure 7 (c)/(d) presents the related line current waveforms and the spectrum. A high content of a 5th and 7th current harmonic is observed leading to unacceptable current waveforms.

Second, the ceDO (tuned to 5th and 7th harmonic voltage rejection) is added to the control loops in the case that the converter side current is measured for the disturbance observer input. Figure 7 (e)/(f) presents the related line current waveforms and the spectrum. The 5th harmonic current is reduced to *25* % and the 7th harmonic current is reduced to *62* % of the harmonic current contents that are measured without the ceDO.

Third, the ceDO (tuned to 5th and 7th harmonic voltage rejection) is added to the control loops where the line side current is measured for the disturbance observer input. Figure 7 (g)/(h) presents the related line current waveforms and the spectrum. A higher reduction of the harmonic current contents is observed in relation to the aforementioned experiments. The 5th harmonic current is reduced to *8* % and the 7th harmonic current is reduced to *38* % of the harmonic current contents that are measured without the ceDO.

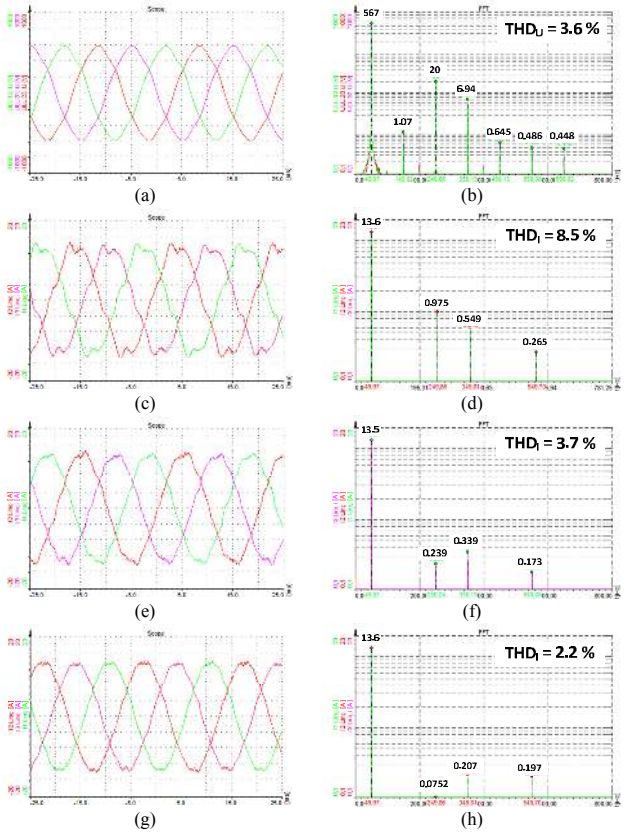

Fig. 7 Measurements results for steady-state voltage disturbance rejection: (a) supply voltage waveforms (line-to-line) and (b) spectrum, (c) line current waveforms without ceDO and (d) spectrum, (e) line current waveforms with ceDO (feedback converter side current) and (f) spectrum, (g) line current waveforms with ceDO (feedback line side current) and (h) spectrum

The presented experimental results demonstrate that the voltage distortion rejection abilities for the measurement of the line side current provide better results in comparison to the case where the converter side current is measured. This is due to the high switching distortion of the converter side current and the resulting harmonic distortion of the measured signals. The line side current waveforms are more efficiently damped by the LCL-filter leading to less distorted measurement signals and an improved ceDO disturbance rejection quality.

B. *Dynamic response*

To study the dynamic distortion rejection abilities of the proposed ceDO another experiment is carried out. In Fig. 8 this experiment is presented for the measurement of the line side current. First, the ceDO (tuned to 5th and 7th harmonic voltage rejection) is disabled and at the time instant $t = 0$ s the ceDO is enabled. The ceDO is able to efficiently reject the voltage disturbances after one fundamental voltage cycle.

VIII. Conclusion

This work presents an extended disturbance observer design for grid voltage disturbance rejection of voltage source PWM converters with LCL filters. The proposed observer design enables the control designer to efficiently reject grid voltage unbalance and lower-order voltage harmonics. The proposed observer design leads to a cascaded extended disturbance observer where the observer design can be based on the feedback of either the converter side current or the line side current. The analysis reveals excellent disturbance rejection abilities for the proposed cascaded extended disturbance observer design for both the feedback cases. However, slightly improved disturbance rejection abilities are observed when the line side current is measured.

Appendix

A. *Calculation of coefficients in the discrete time-domain*

The coefficients of the state-space formulations used in this study are summarized in Table III and Table IV. The overall inductance L_{ges}, the resonance angular frequency ω_{res} and the anti resonance angular frequency ω_0 of the LCL system are derived using (22).

$$L_{ges} = L_c + L_g \qquad \omega_{res} = \sqrt{\frac{L_{ges}}{L_c L_g C_f}} \qquad \omega_0 = \frac{1}{\sqrt{L_c C_f}} \tag{22}$$

B. *Transformation of state-space models from stationary ($\alpha\beta$) into the rotating (dq) reference frame*

Based on the assumption of a (almost) constant line voltage angular frequency ω_{line} the related coefficients in the dq-frame can be derived based on the known coefficients in the $\alpha\beta$-frame using (23)-(30).

$$a_{ij}^{dq} = a_{ij}^{\alpha\beta} e^{-j\omega_{line}T_s} \text{ with } i,j \in [1,2,3] \tag{23}$$

$$a'^{dq}_{ij} = a'^{\alpha\beta}_{ij} e^{-j\omega_{line}T_s} \text{ with } i,j \in [1,2,3] \tag{24}$$

$$b_{ij}^{dq} = b_{ij}^{\alpha\beta} e^{-j\omega_{line}T_s} \text{ with } i \in [1,2,3] \tag{25}$$

$$b'^{dq}_{i} = b'^{\alpha\beta}_{i} e^{-j\omega_{line}T_s} \text{ with } i \in [1,2] \tag{26}$$

$$s_{11}^{dq} = s_{11}^{\alpha\beta} e^{-j\omega_{line}T_s} \tag{27}$$

$$s_{12}^{dq} = s_{12}^{\alpha\beta} \tag{28}$$

$$s_{21}^{dq} = s_{21}^{\alpha\beta} e^{-j2\omega_{line}T_s} \tag{29}$$

$$s_{22}^{dq} = s_{22}^{\alpha\beta} e^{-j\omega_{line}T_s} \tag{30}$$

Acknowledgment

This work is financed by the Ministry of Schleswig-Holstein and the European Union and is operated under Cewind e.G. Center of Excellence for Wind energy Schleswig-Holstein.

TABLE III
COEFFICIENTS OF DISCRETE-TIME LCL STATE SPACE MODEL

$a_{11} = \frac{L_g}{L_{ges}} + \frac{L_c}{L_{ges}}\cos(\omega_{res}T_s)$	$a_{12} = 2\frac{L_c}{L_{ges}}\sin^2\left(\frac{1}{2}\omega_{res}T_s\right)$	$a_{13} = -\frac{\sin(\omega_{res}T_s)}{\omega_{res}L_g}$
$a_{21} = 2\frac{L_g}{L_{ges}}\sin^2\left(\frac{1}{2}\omega_{res}T_s\right)$	$a_{22} = \frac{L_c}{L_{ges}} + \frac{L_g}{L_{ges}}\cos(\omega_{res}T_s)$	$a_{23} = \frac{\sin(\omega_{res}T_s)}{\omega_{res}L_c}$
$a_{31} = \frac{\sin(\omega_{res}T_s)}{\omega_{res}C_f}$	$a_{32} = -\frac{\sin(\omega_{res}T_s)}{\omega_{res}C_f}$	$a_{33} = \cos(\omega_{res}T_s)$
$b_{11} = 0$	$b_{12} = \frac{\sin(\omega_{res}T_s)}{\omega_{res}L_g}$	$b_{21} = -\frac{\sin(\omega_{res}T_s)}{\omega_{res}L_c}$
$b_{22} = 0$	$b_{31} = 2\frac{L_g}{L_{ges}}\sin^2\left(\frac{1}{2}\omega_{res}T_s\right)$	$b_{32} = 2\frac{L_c}{L_{ges}}\sin^2\left(\frac{1}{2}\omega_{res}T_s\right)$

TABLE IV
COEFFICIENTS OF DISCRETE-TIME EXTENDED DISTURBANCE OBSERVER

$s_{11} = \cos(h\,\omega_{line}T_s)$	$s_{12} = \frac{\sin(h\,\omega_{line}T_s)}{h\,\omega_{line}}$	$s_{21} = -h\,\omega_{line}\sin(h\,\omega_{line}T_s)$	
$s_{22} = \cos(h\,\omega_{line}T_s)$	$a'_{11} = \cos(\omega_0 T_s)$	$a'_{12} = \omega_0 C_f \sin(\omega_0 T_s)$	
$a'_{21} = -\omega_0 L_c \sin(\omega_0 T_s)$	$a'_{22} = \cos(\omega_0 T_s)$	$b'_1 = -\omega_0 C_f \sin(\omega_0 T_s)$	$b'_2 = 1 - \cos(\omega_0 T_s)$

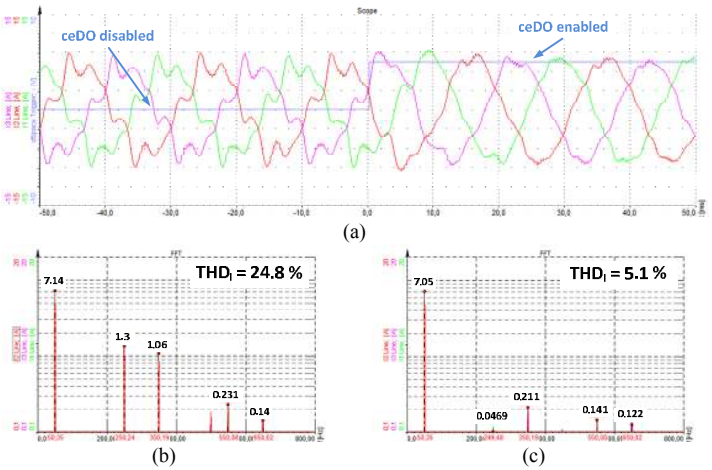

Fig. 8 Measurements results for transient voltage disturbance response using line current feedback: (a) line current waveforms, (b) line current spectrum without ceDO and (c) line current spectrum with ceDO

REFERENCES

[1] R. Wiser and M. Bolinger, "2008 Wind Technologies Market Report," National Renewable Energy Laboratory (NREL), July2009.

[2] "2008 Solar Technologies Market Report," National Renewable Energy Laboratory (NREL), Jan.2010.

[3] A. A. Rockhill, M. Liserre, R. Teodorescu, and P. Rodriguez, "Grid-Filter Design for a Multimegawatt Medium-Voltage Voltage-Source Inverter," *IEEE Trans. Ind. Electron.,* vol. 58, no. 4, pp. 1205-1217, Apr.2011.

[4] B. Bolsens, K. De Brabandere, J. Van den Keybus, J. Driesen, and R. Belmans, "Model-based generation of low distortion currents in grid-coupled PWM-inverters using an LCL output filter," *IEEE Trans. Power Electron.*, vol. 21, no. 4, pp. 1032-1040, July2006.

[5] M. Singh, V. Khadkikar, A. Chandra, and R. K. Varma, "Grid Interconnection of Renewable Energy Sources at the Distribution Level With Power-Quality Improvement Features," *IEEE Trans. Power Del.*, vol. 26, no. 1, pp. 307-315, Jan.2011.

[6] Y. A. Mohamed and M. A. Rahman, "Robust Line-Voltage Sensorless Control and Synchronization of LCL-Filtered Distributed Generation Inverters for High Power Quality Grid Connection," *IEEE Trans. Power Electron.*, vol. PP, no. 99, p. 1, 2000.

[7] H. Jinwei, W. L. Yun, and M. S. Munir, "A Flexible Harmonic Control Approach Through Voltage-Controlled DG-Grid Interfacing Converters," *IEEE Trans. Ind. Electron.*, vol. 59, no. 1, pp. 444-455, Jan.2012.

[8] M. H. J. Bollen, *Understanding Power Quality Problems - Voltages and Interruptions* IEEE Press, 1999.

[9] M. Cichowlas, M. Malinowski, M. P. Kazmierkowski, D. L. Sobczuk, P. Rodriguez, and J. Pou, "Active filtering function of three-phase PWM boost rectifier under different line voltage conditions," *IEEE Trans. Ind. Electron.*, vol. 52, no. 2, pp. 410-419, Apr.2005.

[10] B. Palethorpe, M. Sumner, and D. W. P. Thomas, "System impedance measurement for use with active filter control" *Power Electronics and Variable Speed Drives, 2000. Eighth International Conference on (IEE Conf. Publ. No. 475)*, 2000, pp. 24-28.

[11] A. Tarkiainen, R. Pollanen, M. Niemela, and J. Pyrhonen, "Identification of grid impedance for purposes of voltage feedback active filtering" *IEEE Power Electron. Lett.,* vol. 2, no. 1, pp. 6-10, Mar.2004.

[12] N. Hoffmann, F. W. Fuchs, and L. Asiminoaei, "Online grid-adaptive control and active-filter functionality of PWM-converters to mitigate voltage-unbalances and voltage-harmonics - a control concept based on grid-impedance measurement," in *Proc. Energy Conversion Congress and Exposition (ECCE), 2011 IEEE*, 2011, pp. 3067-3074.

[13] International Electrotechnical Commssion, "Electromagnetic compatibility (EMC) Part 3-2: Limits - Limits for harmonic current emssions, IEC61000-3-2," 2005.

[14] "IEEE Std 529-1992 Recommended Practices and Requirements for Harmonic Control in Electrical Power Systems", 1993.

[15] K. Lee, T. M. Jahns, T. A. Lipo, V. Blasko, and R. D. Lorenz, "Observer-Based Control Methods for Combined Source-Voltage Harmonics and Unbalance Disturbances in PWM Voltage-Source Converters," *IEEE Trans. Ind. Appl.*, vol. 45, no. 6, pp. 2010-2021, Nov.2009.

[16] M. Liserre, R. Teodorescu, and F. Blaabjerg, "Multiple harmonics control for three-phase grid converter systems with the use of PI-RES current controller in a rotating frame," *IEEE Trans. Power Electron.*, vol. 21, no. 3, pp. 836-841, May2006.

[17] P. Rodriguez, J. I. Candela, A. Luna, L. Asiminoaei, R. Teodorescu, and F. Blaabjerg, "Current Harmonics Cancellation in Three-Phase Four-Wire Systems by Using a Four-Branch Star Filtering Topology," *IEEE Trans. Power Electron.*, vol. 24, no. 8, pp. 1939-1950, Aug.2009.

[18] W. Li, D. Pan, X. Ruan, and X. Wang, "A full-feedforward scheme of grid voltages for a three-phase grid-connected inverter with an LCL filter," in *Proc. Energy Conversion Congress and Exposition (ECCE), 2011 IEEE*, 2011, pp. 96-103.

[19] T. Erika and D. G. Holmes, "Grid current regulation of a three-phase voltage source inverter with an LCL input filter," *IEEE Trans. Power Electron.*, vol. 18, no. 3, pp. 888-895, May2003.

[20] P. Van-Tung and L. Hong-Hee, "Control Strategy for Harmonic Elimination in Stand-Alone DFIG Applications With Nonlinear Loads," *IEEE Trans. Power Electron.*, vol. 26, no. 9, pp. 2662-2675, Sept.2011.

[21] VDN Verband der Netzbetreiber, "Technische Regeln zur Beurteilung von Netzrückwirkungen (in german: Technical Rules for System Perturbation Assessment),", 2 ed Frankfurt a.M.: 2007.

[22] M. Malinowski, M. P. Kazmierkowski, S. Hansen, F. Blaabjerg, and G. D. Marques, "Virtual-flux-based direct power control of three-phase PWM rectifiers," *IEEE Trans. Ind. Appl.*, vol. 37, no. 4, pp. 1019-1027, July2001.

[23] C. Chen, C. Desoer, A. Niederlinski, and R. Kalman, "Simplified conditions for controllability and observability of linear time-invariant systems," *IEEE Trans. Autom. Control*, vol. 11, no. 3, pp. 613-614, July1966.